Ultrasonics 97 (2019) 46–56

Contents lists available at ScienceDirect

Ultrasonics

journal homepage: www.elsevier.com/locate/ultras

Experimental and field investigations on seismic response of joints and beddings in rocks

Yang Liu[a], Cai-Ping Lu[a,b,*], Bin Liu[c], Heng Zhang[a], Hong-Yu Wang[d]

[a] Key Laboratory of Deep Coal Resource Mining (Ministry of Education), School of Mines, China University of Mining and Technology, Xuzhou, Jiangsu 221116, PR China
[b] Department of Civil Engineering and Lassonde Institute, University of Toronto, Toronto, Ontario M5S 1A4, Canada
[c] Institute of Rock and Soil Mechanics, Chinese Academy of Sciences, Wuhan, Hubei 430071, PR China
[d] Department of Civil, Environmental and Mining Engineering, School of Engineering, University of Western Australia, Crawley, WA 6009, Australia

ARTICLE INFO

Keywords:
Joints and beddings
Stress
Seismic attenuation
Wave velocity
Frequency-spectrum evolution

ABSTRACT

Based on experimental and in-situ tests, the propagation and attenuation rules of seismic wave in the intact and jointed rocks subjected to conventional triaxial loading condition were investigated, especially the influencing effects of joints and beddings on the attenuation. Meanwhile, the frequency-spectrum evolutions during the process of attenuation were analysed in detail. To verify the outcomes obtained from the laboratory, the attenuation characteristics of seismic wave generated by blasting in underground strata were tested, and the attenuation rules by the joints between strata was summarized. Finally, the seismic response of joints and beddings in rocks was revealed. This work put forward some references for early weakening and controlling coal-rock dynamic disasters triggered by seismic wave in coal mines based on the attenuation effect of artificial discontinuity such as joint and bedding.

1. Introduction

Fractured rocks significantly influence the geotechnical stability of a site, and the heterogeneities on different scales, such as fractures, joints and micro-cracks, can vary, or are altered by artificial interferences. As the physical properties of discontinuities change in time, active monitoring techniques should be improved to quantify the variations in the fractured rocks. It is well known that microseism (MS) and acoustic emission (AE) can accurately locate fractures and characterize the mechanical properties of fractured rocks, but the further development was hampered due to the lack of understanding of the relationships and interaction among the physical properties of fractures. Recently, some attempts have been conducted to investigate and reveal the physical properties of fractures including seismic response based on field and laboratory studies.

An initial fracture in rock consists of two contact rough surfaces. From elasticity, the mechanical stiffness of a fracture depends on the spatial distribution and the amount of contact area within a fracture [1–4]. Seismic wave propagation has been shown to be sensitive to both the normal and shear stiffness across a fracture, and also the pore fluids contained within the fracture [5–11]. Traditionally, wave propagation through a fracture/or joint has been modelled by using effective medium theories. For example, Gaviglio established the relationship between wave velocity and medium density [12]. Pyrak-Nolte et al. derived a theoretical velocity based on the displacement discontinuity model of wave propagation across a fracture [13]. Zhao et al. developed an equivalent medium method to explain wave phenomena [14]. Wang et al. investigated the far-field blast-wave propagation and attenuation in rock shelter layer with an inclusion or filled medium [15]. Zakian et al. used a stochastically enriched spectral finite element method (StSFEM) to solve wave propagation problems in random media [16]. Li et al. employed a thin-layer interface model for filled rock joints to analyse wave propagation across the jointed rock masses [17,18]. Wu et al. found that the stress discontinuity in a rock fracture largely depended on the existence of filling materials which promoted the P-wave attenuation and the decrease of fracture stiffness [19]. Cai and Zhao established a numerical modelling on the effects of multiple parallel planar fractures on the attenuation of normally incident one-dimensional elastic waves [20]. Mashinskii found that the wave attenuation was improved by inclusion in the seismic rheological model [21]. Fan et al. proposed a nonlinear viscoelastic equivalent medium model for longitudinal stress wave propagation in a rock mass, and found that wave propagation in complex rock masses was not always attenuated but may actually be enhanced in some cases [22–24]. Ma et al.

* Corresponding author at: Key Laboratory of Deep Coal Resource Mining (Ministry of Education), School of Mines, China University of Mining and Technology, Xuzhou, Jiangsu 221116, PR China.
E-mail address: cplu@cumt.edu.cn (C.-P. Lu).

https://doi.org/10.1016/j.ultras.2019.05.001
Received 17 February 2019; Received in revised form 3 April 2019; Accepted 3 May 2019
Available online 03 May 2019
0041-624X/

evaluated the existing equivalent medium methods for jointed rock mass and further developed the equivalent viscoelastic medium method [25].

As summarized above, the mechanical characteristics of a fractured rock with discontinuities have been extensively investigated, and the propagation and attenuation rules of seismic wave through a fracture with different mechanical properties have been also clearly revealed. However, even though the attenuation rules generated by joint have been fruitfully investigated in lab, limited attention has been paid to characterizing the attenuation effect of seismic wave by bedding and coupled attenuation by both joint and bedding Thus, understanding the coupled attenuation effect by both beddings and joints using a triaxial acoustic P-S1-S2 system and identifying the frequency-spectrum evolution of seismic wave is of vital importance.

In this paper, we first presented a survey of our current understanding of these interrelationships wave velocity, frequency-spectrum distribution and discontinuities including bedding and joint based on experimental and in-situ tests. Secondly, the attenuation differences by joint and bedding in rocks were discussed in detail. Furthermore, the outcomes obtained from experiments were verified from the field investigation.

2. Experimental measurements of seismic waves

2.1. Test apparatus

The test facilities at the Lassonde Institute of Mining, University of Toronto were used and a Hoek type triaxial cell with axial linear variable differential transformers (LVDTs) and data acquisition module (as shown in Fig. 1(a)) was employed for this tests. This system includes the ErgoTech variable pulse width transducer, and the pulser unit with a variable pulse width range of 100–1000 ns P-S1-S2 wave on axial load applying platens is controlled manually using the transducer pulser unit, and the amplitude and frequency of the source was set to 100 V and 5×10^7 Hz, respectively. At each stage during the test, the vertical stress was approximately equivalent to the confining stress. Fig. 1 shows the photos of the testing system and three samples.

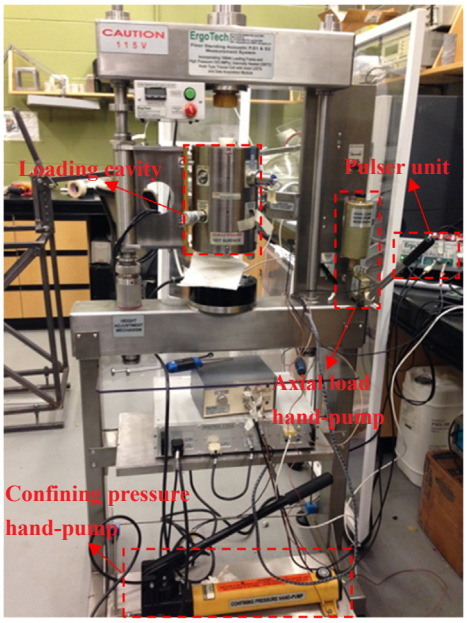

(a) Triaxial acoustic P-S1-S2 system

(b) #1 sample

(c) #2 sample

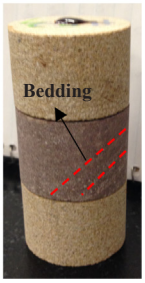

(d) #3 sample

Fig. 1. Photos of the testing system and three samples. Notes: The #1 sample is intact, the #2 sample has two horizontal joints, and the central part of the #3 sample incorporates beddings besides two joints.

2.2. Samples

In total, three sandstone samples were prepared, with dimension of 35 mm in diameter and 78 mm in height, and with two joints oriented orthogonal to the long axis of the core except the #1 sample. They were tested to investigate the wave velocity and seismic responses of joints and beddings. The three samples were processed from two types of sandstone with the uniaxial compressive strength (UCS) of 52.63 MPa and 57.32 MPa, and the modulus of elasticity of 17.86 GPa and 21.35 GPa, respectively. As for the seismic measurements, the intact #1 sample, which was taken immediately adjacent to the jointed samples from the same core, was also tested to provide references and comparison. Table 1 shows the physical and mechanical parameters of each sample.

2.3. Seismic results

2.3.1. Influencing effects of joints on wave velocity

Fig. 2 shows the complete waveforms and first-motion times of P & S1-wave recorded by the receiving geophone of the three samples when the axial vertical stress is 20 MPa.

From Fig. 2, the effect of two joints on seismic wave attenuation can be observed in data. By comparing the three signals, three effects of joints and beddings on P & S1- wave were observed: (i) the joints and beddings delay the signal according to the first motion times of P & S1-wave; (ii) the joints and bedding attenuate the signal based on the amplitude of receiving waves; and (iii) the joints and beddings weak the high frequency components of the signals, especially for the compressional P-wave. This attenuation mechanism of beddings in rock on seismic wave was rarely reported in the literature. By comparing the testing results between #2 and #3 samples, it was found that the amplitude of P & S1-wave was significantly reduced by the beddings while its effect on wave velocity was not obvious.

Fig. 3 shows the variations of the receiving P & S-wave velocities with axial stress level of the three samples.

Based on previous investigations, the effect of the joint is distributed throughout the bulk and the discreteness of the joint is lost. Therefore, a seismic reduction in velocity is observed. In Fig. 3, the P- S1- S2-wave velocities of the #2 and #3 samples were significantly reduced compared with the intact #1 sample due to the existence of the joints. Interestingly, the differences of the three velocities between them were small, confirming that the influencing effect of the bedding on wave velocity was not obvious. Because of the existence of the bedding in the #3 sample, the P-wave velocity of the #2 sample was larger than that of the #3 sample, when the axial stress surpassed 10 MPa. However, the S-wave velocity of the former was slightly lower than that of the latter one, which was possibly due to the effect of lithology of the #3 sample on S-wave velocity partially offset the attenuation effect of the bedding. In addition, the P & S-wave velocities rose with the increase of the axial stress, and the increment of the velocities decreased gradually, especially for the intact sample (#1 sample), this trend was the most obvious. Previous studies have found that wave velocity was influenced by stress and the damage state of rocks [26–30].

Table 1
Physical and mechanical parameters of each sample.

Sample No.	Height (up: centre: bottom)/mm	Diameter/mm	Maximum axial stress/MPa
#1	78.1	35.85	30
#2	78.07 (26.49: 25.46: 26.12)	35.93	50
#3	77.42 (25.49: 26.72: 25.21)	35.90	60

In order to describe the relationship between stress and seismic wave velocity in rocks, the following empirical expression has been summarized using a large number of experiments [31].

$$V = V_0 + D \cdot P - B \cdot e^{-k \cdot P} \quad (1)$$

where V is the wave velocity with some fractures: P-wave velocity (V_P) or S-wave velocity (V_S); P is the effective stress applied to rock; V_0 is the wave velocity without fracture: P-wave velocity (V_{P0}) or S-wave velocity (V_{S0}); and B, D, and k are fitting parameters. D is often left as zero as it can result in unreasonable values at elevated stresses [32].

2.3.2. Attenuation effects of stress on wave spectrum

The propagation and attenuation effects of single fracture on seismic wave have been verified fruitfully both in lab and by field tests. However, how seismic waves respond needs further experimental investigations considering double influencing factors including stress and joints.

(1) The intact #1 sample without cracks

Based on the Fast Fourier Transformation (FFT) of seismic signals, the frequency-spectrum evolutions of P & S1-wave of the #1 sample with different axial stress were analysed, as shown in Fig. 4.

Based on spectrum analysis, the frequency-spectrum distribution characteristics of S1 & S2-wave were basically similar. Therefore, we only discuss the S1-wave here. From Fig. 4(a), the frequency-spectrum distribution of P-wave did not change significantly with the increase of axial stress, while the high-frequency parts increased first and then decreased slightly, while the low-frequency parts kept increasing. This phenomenon may be attributed to the fact that the signals of receiving waves were enhanced due to the weak attenuation caused by the stress increase. The amplitude spectrum of dominant high frequencies at 20 MPa was higher than that at 30 MPa, however, the high-frequency components of the latter were more abundant and the overall signal was stronger, verifying that the higher the stress is, the weaker the attenuation of signal is, and the abundant the high frequency is. In addition, the attenuation of P-wave was obvious, and the low-frequency signal was stronger with wide frequency band. However, the high-frequency components were still dominant. According to Fig. 4(b), the attenuation of S-wave was not obvious, and the spectrum was mainly

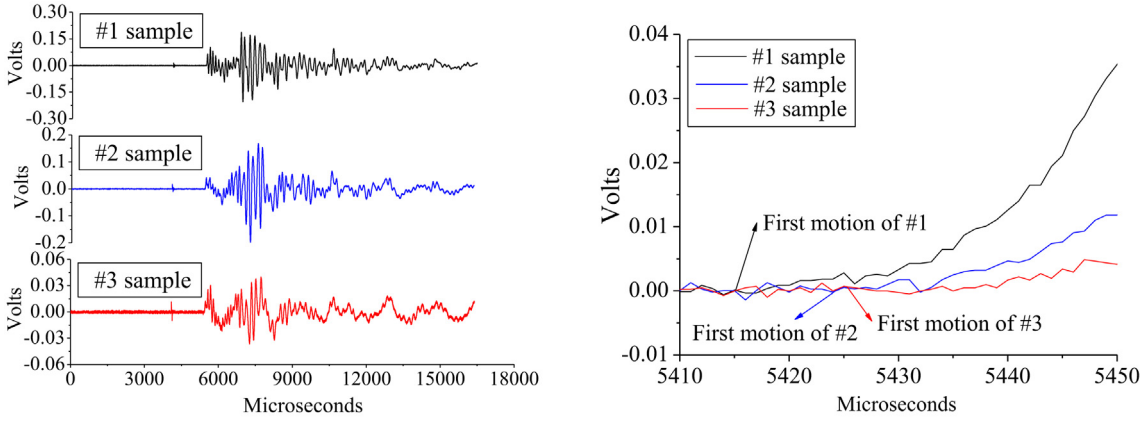

(a) Waveforms and first motions of P-wave

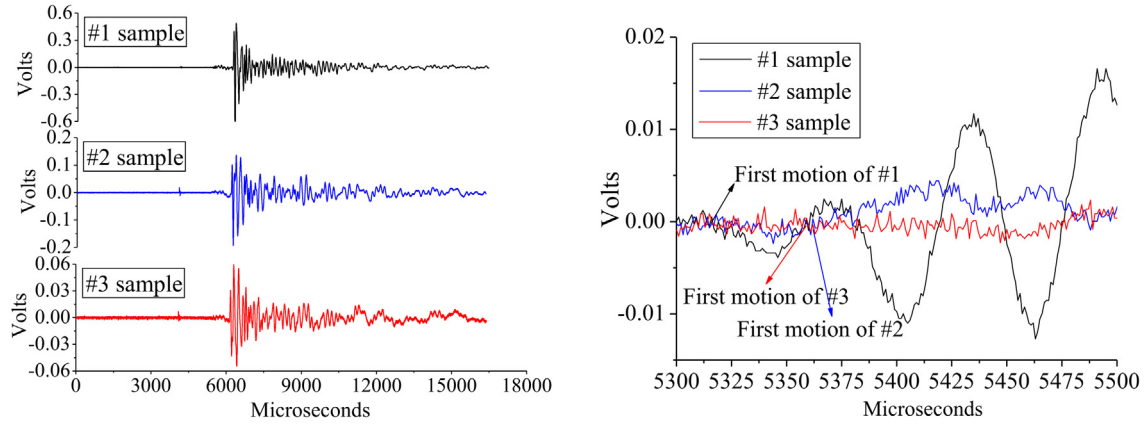

(b) Waveforms and first motions of S1-wave

Fig. 2. Comparisons of P and S1-wave propagated through an intact sample and two jointed samples subjected to both vertical stress of 20 MPa and confining stress of 20 MPa.

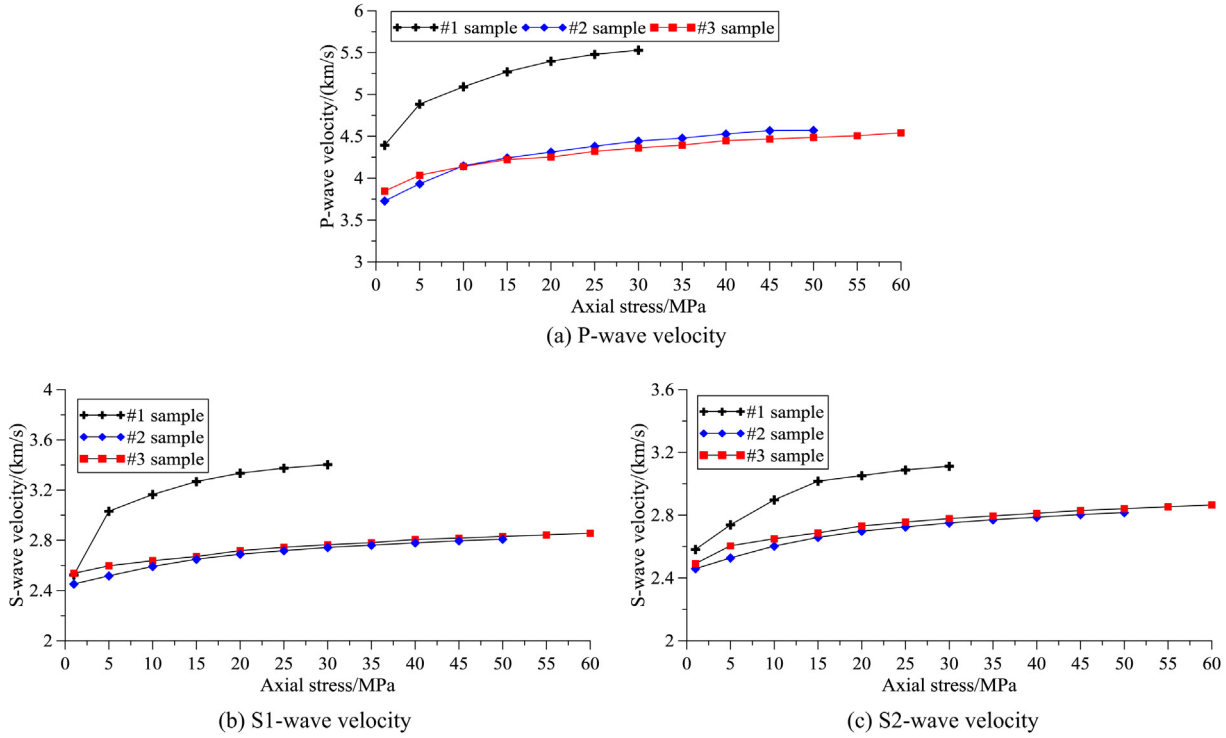

Fig. 3. Variations of P & S-wave velocities with axial stress level of the three samples.

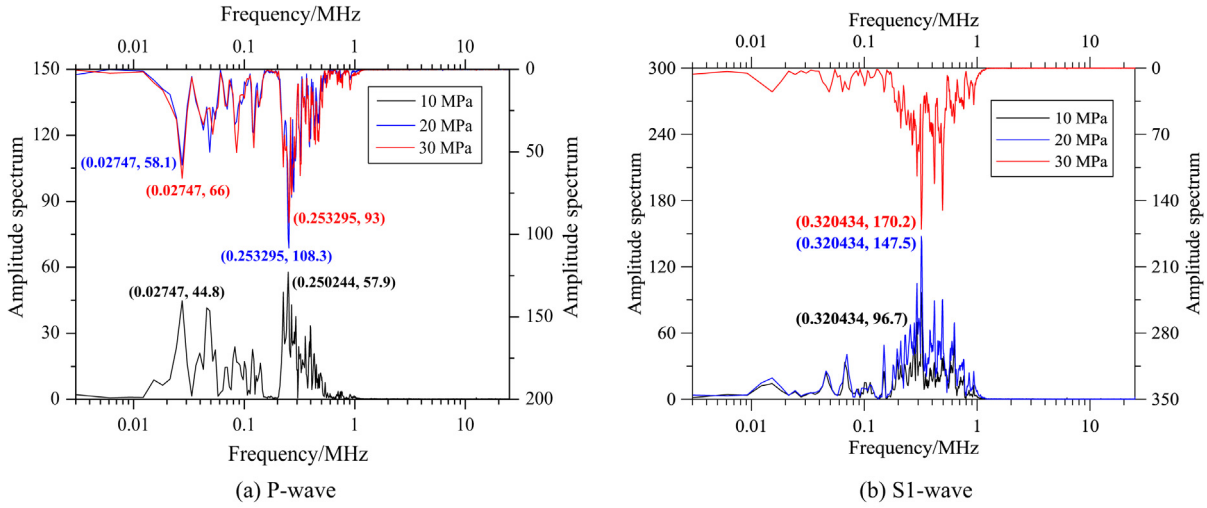

Fig. 4. Frequency-spectrum evolutions of P & S1-wave of the #1 sample with different axial stress.

distributed in the high frequency range. With the increase of axial stress, the signal was gradually strengthened.

(2) The jointed #2 sample with two joints

Fig. 5 shows the frequency-spectrum evolutions of P & S1-wave of the #2 sample with different axial stress.

From Fig. 5(a), the joints between rocks further attenuated the P-wave compared with the #1 sample, and the low-frequency signals were significantly enhanced. The structural plane of the joints was compacted gradually with the increase of axial stress, and therefore the attenuation effect on P-wave was weakened. Meanwhile, the low frequency signals gradually strengthened. Although the amplitude spectrum of dominant high frequency increased first and then reduced, the frequency corresponding to the peak amplitude spectrum reached up to 0.311 MHz at 50 MPa, and the high frequency components were abundant compared to 30 MPa, indicating that the higher the stress is, the weaker the attenuation of seismic wave is, the more abundant the high frequency components are, and the higher the dominant frequency is. From Fig. 5(b), the attenuation effect of the horizontal joints on S-wave was not obvious, and thus the signals still manifested themselves in the form dominant high frequency. The higher the axial stress is, the larger the amplitude spectrum corresponding to dominant high frequency is, and the more abundant the high frequency components are.

(3) The jointed #3 sample with two joints and beddings

Fig. 6 shows the frequency-spectrum evolutions of P & S1-wave of the #3 sample with different axial stress.

From Fig. 6(a), the frequency-spectrum of the #3 sample

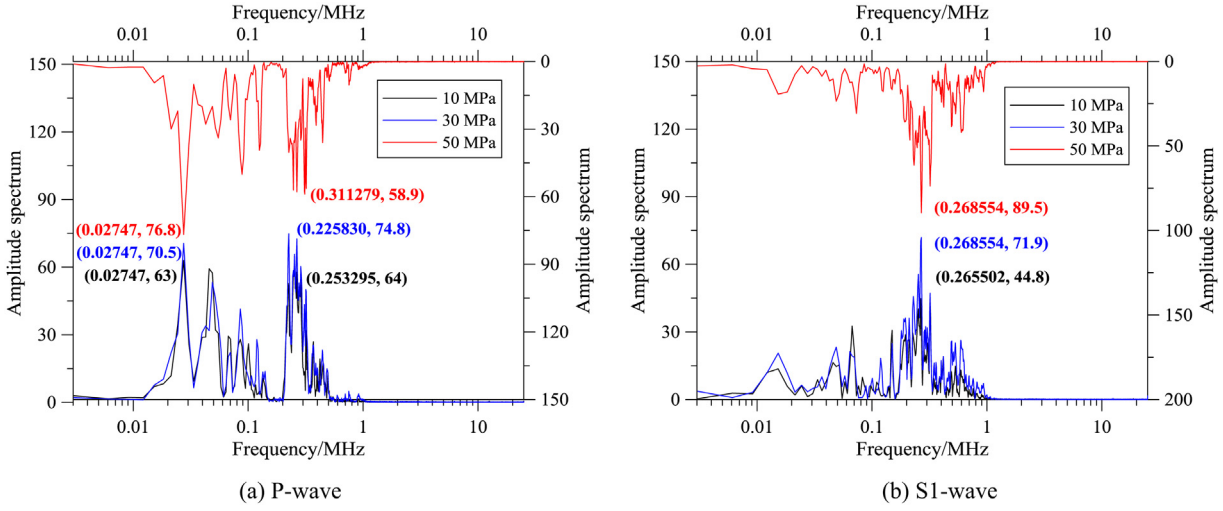

Fig. 5. Frequency-spectrum evolutions of P & S1-wave of the #2 sample with different axial stress.

dominantly concentrated in the low-frequency band compared with that of the #2 sample, and the high frequency components decreased significantly, indicating that the bedding further reduced P-wave on the basis of the attenuation effect of the joints and the dominant frequency obviously moved from high-frequency 0.253 MHz to low-frequency 0.0275 MHz. When the stress reached 10 MPa, the spectrum presented wide frequency and the high frequency signals were stronger. However, when the stress was larger than 20 MPa, the spectrum moved obviously to the low frequency band, and the amplitude spectrum corresponding to the dominant low frequency increased gradually, which may be related to deformation and fracture of the beddings equivalently generating new joints and thus the attenuation of P-wave was strengthened. From Fig. 6(b), the spectrum of S1-wave obviously concentrated in the low frequency band when the stress was 20 MPa, also verifying deformation and fracture of the beddings. With the increase of stress, the spectrum of S1-wave manifested wide frequency, and the dominant frequency moved to the low frequency band, accompanied with abundant high frequency components, indicating that the inclined beddings have a certain attenuation effect on S-wave.

To sum up, it was found that as stress on the jointed sample was increased, the amount of energy transmitted across the joint increased, which was observed as an increase in magnitude or the spectral peak of seismic wave. In addition, the spectral peak shifted to higher frequency with the increase of the axial stress. However, the macroscopic joints produced significant attenuation effect on the P-wave, and the spectral peak was converted from high to low frequencies. The inclined beddings attenuated the S-wave to a certain extent, and the spectrum manifested wide frequency with abundant low frequency components. As stress on the jointed sample increased, the joint stiffness increased, resulting in an increase in transmission across the joint, and thus the receiving wave manifested abundant high-frequency characteristics. At very high stresses, the joint behaves similar to that of the intact sample. In contrast, the slip and fracture may be produced along the inclined beddings under high stress, which will strengthen the attenuation effect on seismic wave.

2.3.3. *Attenuation effects of joints on wave spectrum*

Both in-situ and laboratory investigations on artificially and naturally fractured rocks have shown that they exhibit frequency-dependent transmission losses [33–37]. Generally, a fracture behaves as a low-pass filter that attenuates the high-frequency components of signals. However, what are the differences between the attenuation characteristics of P and S-wave by joints and beddings? Which has stronger attenuation effect? The role of stress in attenuation process on seismic wave for the jointed samples should be further investigated in lab.

Fig. 7 shows the frequency-spectrum evolutions of P-wave and variations of spectral peaks corresponding to high and low frequencies of the three samples with different stresses.

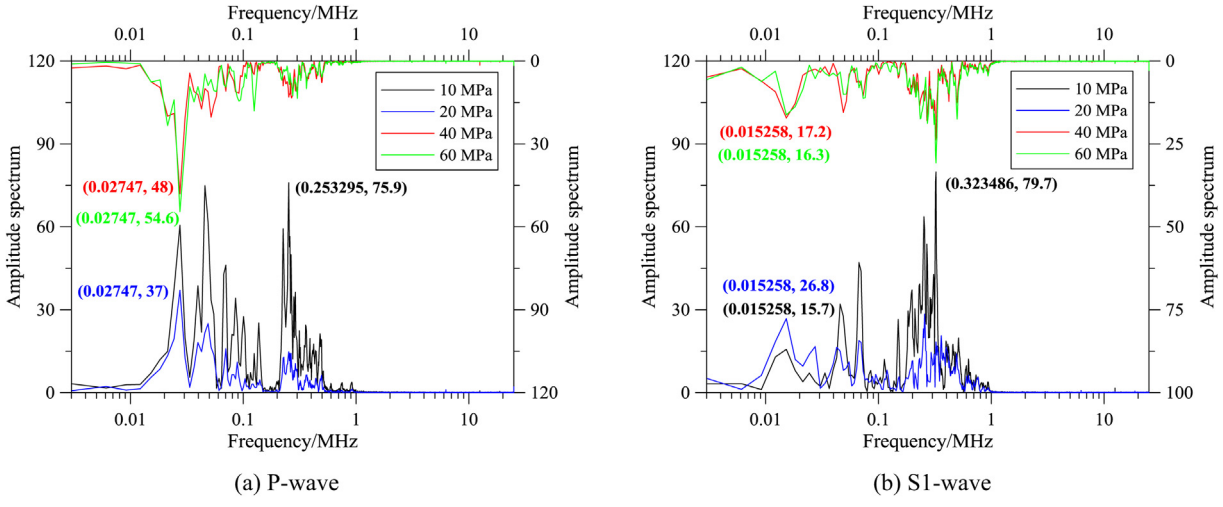

Fig. 6. Frequency-spectrum evolutions of P & S1-wave of the #3 sample with different axial stress.

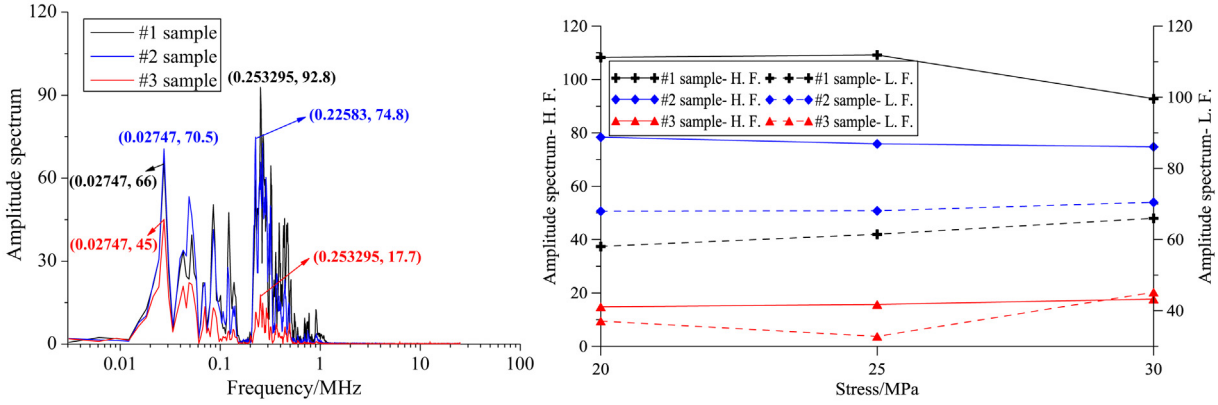

(a) Stress= 30 MPa (b) Spectral peaks

Fig. 7. Frequency-spectrum evolutions of P-wave and variations of spectral peaks corresponding to high and low frequencies with different stresses. Note: in the legend of subgraph (b), H. F. and L. F. represent dominant high and low frequencies, respectively.

From Fig. 7(a), the joints of the #2 sample obviously attenuated the high-frequency signals of P-wave and enhanced the low-frequency components, while the spectrum still presented wide-frequency characteristics. Due to the existence of the beddings, the amplitude of high-frequency signal of the #3 sample decreased significantly, and the spectrum was concentrated in the low frequency band. Meanwhile, the amplitude spectrum corresponding to dominant low frequency was obviously lower than that of the #2 sample due to the attenuation effect of the beddings, and especially the attenuation coefficient of high-frequency signals reached 5.24. From Fig. 7(b), the attenuation effect of stress on the P-wave of the fractured sample was not significant based on the variations of amplitude spectrum corresponding to dominant high and low frequencies with stress.

Fig. 8 shows the frequency-spectrum distributions of the receiving S2-wave and the variations of spectral peaks corresponding to dominant high and low frequencies of the three samples with different stress levels.

From Fig. 8(a), the joints obviously attenuated the high frequency band of S2-wave instead of low frequency signals. The beddings further attenuated the high-frequency signals. The amplitude spectrum corresponding to dominant high frequency was reduced, while the attenuation of low frequency signals was not obvious. From Fig. 8(b), the effect of stress on the high-frequency signals of S-wave of intact sample is significant. The higher the stress was, the weaker the attenuation effect was, and the larger the amplitude corresponding to dominant high frequency was. Especially, the effect of stress on low-frequency components was slight, and the attenuation effect on S-wave of fractured sample was also not obvious.

2.3.4. *Attenuation effects of beddings on wave spectrum*

The displacement discontinuity structure yields transmission and reflection coefficients that depend on the specific stiffness of the structure, k, the seismic impedance of the half-spaces Z and the frequency content of the signal, ω [37]. The beddings in the #3 sample also belong to one kind of displacement discontinuity structure. What are the differences of the attenuation characteristics on seismic wave between the bedding and joint?

Fig. 9 shows the frequency-spectrum distributions of the receiving P-wave and variations of spectral peaks corresponding to dominant high and low frequencies of the #2 and #3 samples at different stresses.

From Fig. 9(a), the bedding of the #3 sample further attenuated the P-wave after propagating through joints, and the high-frequency signals were significantly weakened with dominant low frequency characteristics. Due to the attenuation effect of the beddings, the amplitude spectrum corresponding to dominant low frequency of the #3 sample was smaller than that of the #2 sample. From Fig. 9(b), with the increase of axial stress, the dominant high-frequency signals of P-wave of the #3 sample were basically stable, but the dominant low-frequency signals obviously enhanced, indicating that the higher the stress is, the weaker the attenuation effect of bedding is, and the low-frequency signals are stronger. For the #2 sample, the increasing stress caused the reduction of the dominant high frequency signals, which may be related

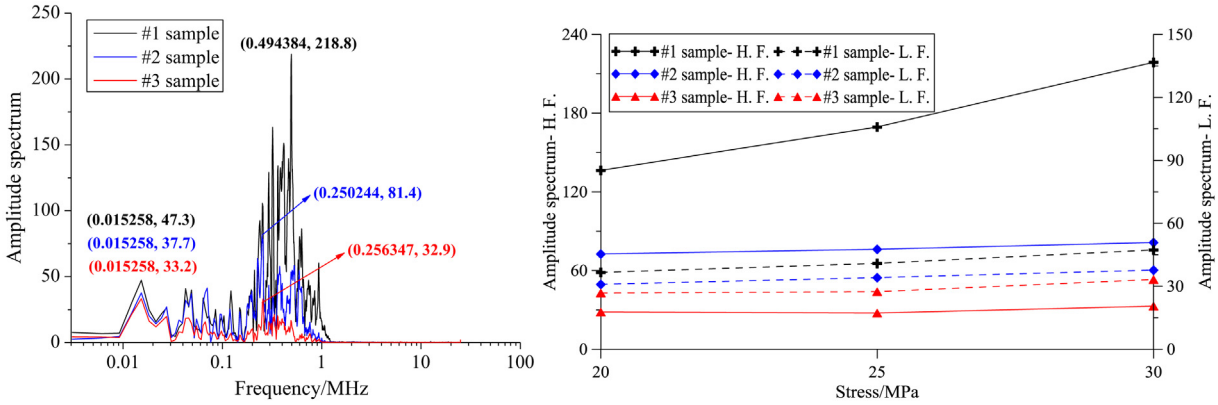

(a) Stress= 30 MPa (b) Variations of spectral peaks with stress

Fig. 8. Frequency-spectrum distributions of S2-wave and the variations of spectral peaks corresponding to dominant high and low frequencies of the three samples with stress. Note: in the legend of subgraph (b), H. F. and L. F. represent dominant high and low frequencies, respectively.

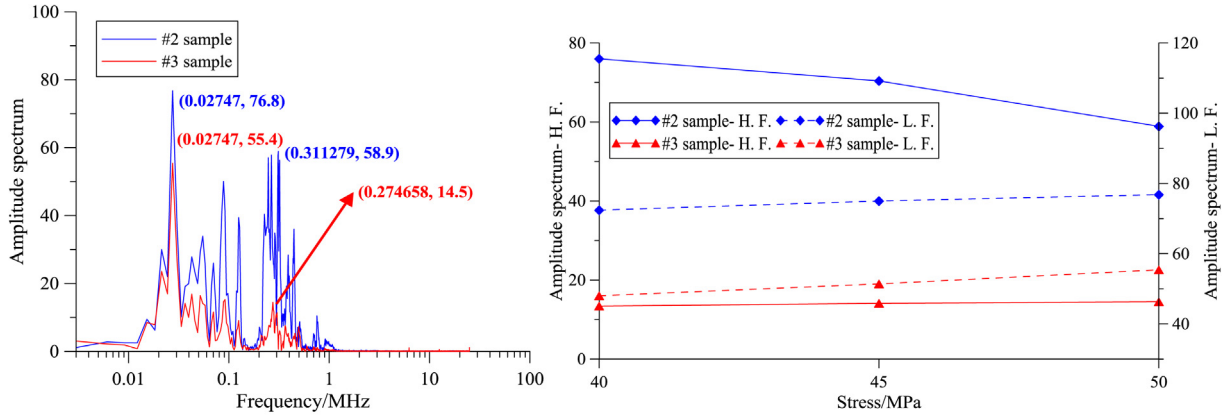

(a) Stress= 50 MPa (b) spectral peaks

Fig. 9. Frequency-spectrum distributions of P-wave and variations of spectral peaks corresponding to dominant high and low frequencies of the #2 and #3 samples. Note: in the legend of subgraph (b), H. F. and L. F. represent dominant high and low frequencies, respectively.

to the failure of joints under high stress resulting in obvious attenuation of high frequency signals and the shift of spectrum from high to low frequency band. Meanwhile, the low frequency signals were enhanced.

Fig. 10 shows the frequency-spectrum distributions of the receiving S2-wave and variations of spectral peaks corresponding to dominant high and low frequencies of the #2 and #3 samples at different stresses.

From Fig. 10(a), the attenuation effect of the beddings on S-wave was weaker than the effect on P-wave, the attenuation coefficients of amplitude spectrum corresponding to dominant high and low frequencies obviously reduced, and the dominant high frequencies decreased correspondingly. Meanwhile, the spectrum distribution of the #3 sample manifested wide frequency and the high-frequency signals were stronger. Compared with Fig. 9(a), the attenuation effect of beddings on P-wave was stronger than that on S wave. From Fig. 10(b), the effect of stress on seismic wave attenuation for the jointed rock was not obvious.

When the fracture stiffness approaches 0 ($k \rightarrow 0$), the transmission coefficient reduces to 0 and the reflection coefficient rises to 1. Therefore, the fracture acts as a free surface, which contributes to the extensive crack growth [37]. Conversely, as the fracture stiffness approaches infinity ($k \rightarrow \infty$), the fracture acts as a welded contact for which all of the energy is transmitted across the fracture without energy partitioned into the reflected signal [38]. In addition, from the crack growth point of view, the contact surfaces of the initial fractures are strong driver of subsequent crack growth [39].

The following four points were summarized: (1) the attenuation of horizontal joints on seismic wave velocity is very significant, but that of inclined beddings is not obvious, especially for S-wave; (2) for the intact sample, the P-wave attenuation is obvious, and the low-frequency signal is strong. The attenuation of S-wave is not obvious, and the spectrum mainly distributes in the high-frequency band. For the jointed sample, the attenuation of P-wave is significant, and the low-frequency signal is enhanced. However, the attenuation of S-wave is not obvious manifesting dominantly high-frequency characteristics. On the basis of joint, the bedding further attenuates the P-wave, while the attenuation effect for S-wave is relatively weak. When the stress is high, the beddings may generate slip and fracture, which is equivalent to forming new joints aggravating the attenuation; (3) the joints attenuate the high-frequency signals of P-wave, and the low frequency components are enhanced. However, the spectrum still shows wide frequency characteristics. The attenuation of S-wave mainly concentrates in high frequency band, and that of low frequency is not obvious. The beddings further attenuate the P-wave after propagating through joints, and thus the high frequency signals are weakened significantly with low frequency characteristics. The attenuation of the beddings on S-wave is weaker than that on P-wave, and the attenuation index decreases significantly; and (4) for the intact sample, the higher the stress is, the weaker the attenuation of signal is, and the high frequency is more abundant. For the jointed sample, the attenuation effect of stress on both P and S-wave is not obvious.

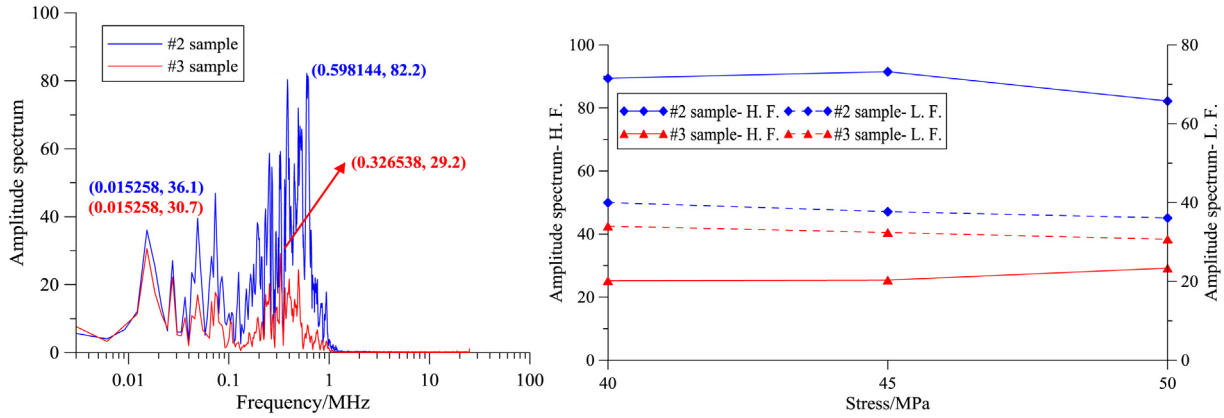

(a) Stress= 50 MPa (b) Spectral peaks

Fig. 10. Frequency-spectrum distributions of S2-wave and variations of spectral peaks corresponding to dominant high and low frequencies of the #2 and #3 samples. Note: in the legend of subgraph (b), H. F. and L. F. represent dominant high and low frequencies, respectively.

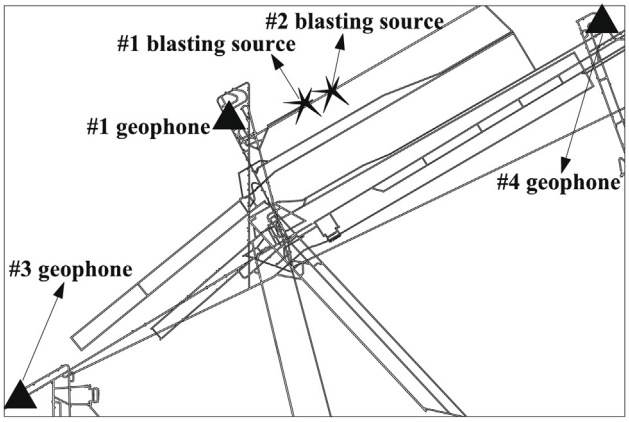

Fig.11. The distributions of blasting sources and the geophones.

3. Field observation of seismic attenuation characteristics with joints.

3.1. In-situ testing conditions

Field investigation on propagation and attenuation effects of joints between rock layers on seismic wave generated by blasting was carried out in a tailentry of a working face characterized by strong rockburst danger. The average elevation of the tailentry was approximately −840 m, and total of three three-component geophones named as #1, #3 and #4 were arranged around the tailentry. The frequency response of the geophone is 5–500 Hz, and the sampling rate is 1000 sps. The absolute time error of GPS clock is less than 1 ms with trigger recording mode, and seismic events with M_L of 0.5–4.5 in the effective monitoring area can be recorded clearly by lower threshold. Because the tailentry was being excavated, the seismic waves generated by blasting after propagation and attenuation through coal and rock medium were collected by the #1, #3 and #4 geophones arranged in different rock layers, and the distributions of blasting sources and the geophones are shown in Fig. 11. Based on the three geophones, the attenuation characteristics of joint between rock layers on the P and S-wave can be analysed in detail. Table 2 shows the three-dimensional coordinates of the three geophones and the Table 3 shows the strata and joints distribution in the testing area.

From Table 3, the vertical distances between the blasting source and the #1, #3 and #4 geophones were 42.2 m, 125.5 m and 117.84 m, and the corresponding number of joints between them was 5, 8 and 7, respectively. The working faces and roadways were all located #7 coal seam, therefore, only intact coal and rock mass located along straight line direction between blasting source and the geophones according to Fig. 11 and Table 3

3.2. Testing results and analysis

(1) In-situ test 1: After blasting with five blast holes and total explosive charge of 15 kg in the tailentry, the clear seismic waveforms were received and recorded by the three geophones. The propagation distances of the seismic wave to the explosive source to the #1, #3 and #4 geophones were 249.5 m, 1306 m and 986.6 m, respectively. Fig. 12 shows the waveforms and first arrival times of the P-wave recorded by the three geophones and the Fig. 13 shows the frequency-spectrum distributions of the P and S-wave.

Table 2
Three-dimensional coordinates of #1, #3 and #4 geophones.

Geophone No.	X/m	Y/m	Z/m
#1	3864466.831	39478794.5	−902.2
#3	3863577.653	39478134.35	−734.5
#4	3864772.992	39479980.53	−742.157

Table 3
Distribution of strata and joints in the testing area.

Mineral No.	Lithology	Thickness/m	Notes
1	Mudstone	30–45	#3 geophone
2	Siltstone	40	#4 geophone
3	Sandstone	10	
4	Mid-coarse sandstone	30	
5	Sandstone	15	
6	Silt and fine sandstone	5	
7	Mid-fine sandstone	14	
8	Siltstone	3	
9	#7 coal seam	1.8	Blasting source (−860 m)
10	Siltstone and mudstone	3.5	
11	Medium sandstone	22	
12	#9 coal seam	2.2	
13	Fine sandstone	10	
14	Sandstone	10	#1 geophone

From Fig. 12(a), with propagation away from the blasting source, the high-frequency signals of the P-wave obviously weakened, and the low-frequency signals relatively enhanced. According to Fig. 12(b), the farther the propagation distance of seismic wave is, the later the first arrival time of P-wave is. For example, the propagation distance from the source to #1 geophone was only 249.5 m, and the first arrival time of the P-wave was much earlier than that of #3 and #4 geophones.

From Fig. 13(a), with the increase of vertical propagation distance, the high frequency signals of P-wave attenuated significantly, the dominant frequency decreased from 190 Hz to 28 Hz, and the spectrum moved from high frequency to low frequency band. In particular, the vertical propagation distance of the #3 geophone increased only 7.66 m and experienced one more joint compared with the #4 geophone, while the amplitude spectrum corresponding to dominant frequency reduced by nearly 2.5 times, which fully demonstrated the significant attenuation effect of joints on P-wave. From Fig. 13(b), with the increase of horizontal propagation distance, the high frequency signals of S-wave attenuated significantly, and the dominant frequency of S1-wave and S2-wave decreased from 194.8 Hz to 25 Hz, and 194 Hz to 29 Hz, respectively. The horizontal distances from the source to the #3 and #4 geophones were 1300 m and 980 m, respectively, with a difference of up to 320 m, while the dominant low frequencies of them were very close, and their corresponding amplitude spectra were almost equivalent, indicating that the attenuation effect of the horizontal joints on S-wave was not obvious, which was consistent with the observations in lab. In addition, the horizontal propagation distance of the #3 geophone to the source was 5.3 times that of the #1 geophone, the amplitude spectrum corresponding to dominant frequency reduced nearly 6.5 times. However, the vertical propagation distance of the former increased by 3 times compared with the latter, the amplitude spectrum corresponding to dominant frequency reduced by nearly 10.7 times, which fully proved the significant attenuation effect of the joints on P-wave.

(2) In-situ test 2: After blasting with six blast holes and total explosive charge of 15 kg in the tailentry, the clear seismic waveforms were received and recorded by the three geophones. The propagation distances of #1, #3 and #4 geophones to the explosive source were 315 m, 1371.5 m, and 920 m, respectively. Fig. 14 shows the waveforms of S1-wave collected by the three geophones and the corresponding first arrival times and the Fig. 15 shows the frequency-spectrum distributions of P and S-wave.

Totally, the results of the second test were similar to that of the first

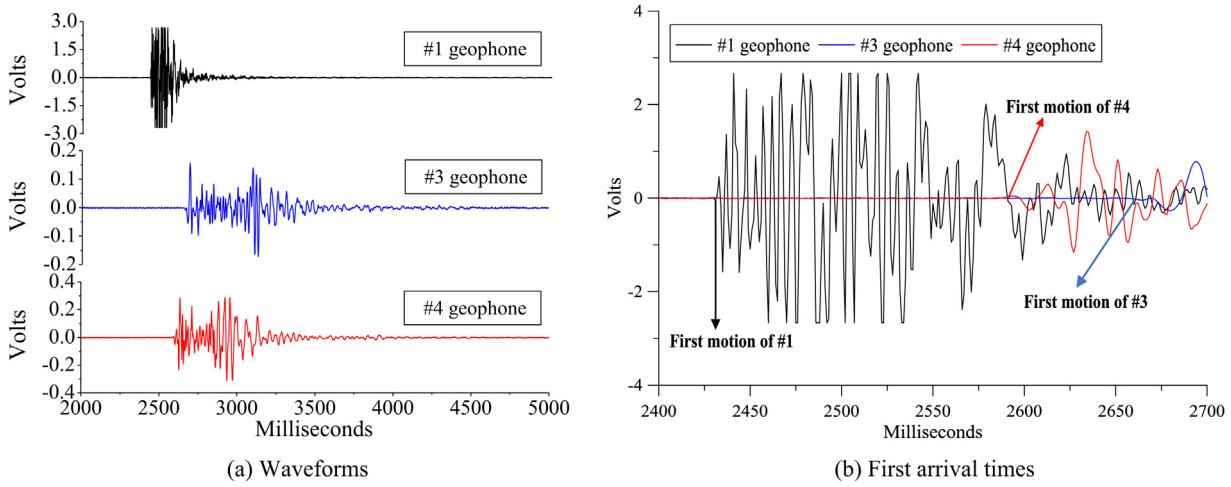

Fig. 12. Waveforms and first arrival times of the P-wave recorded by the #1, #3 and #4 geophones. Note: in the subgraph (b), the amplitudes of both #3 and #4 geophones were magnified 5 times.

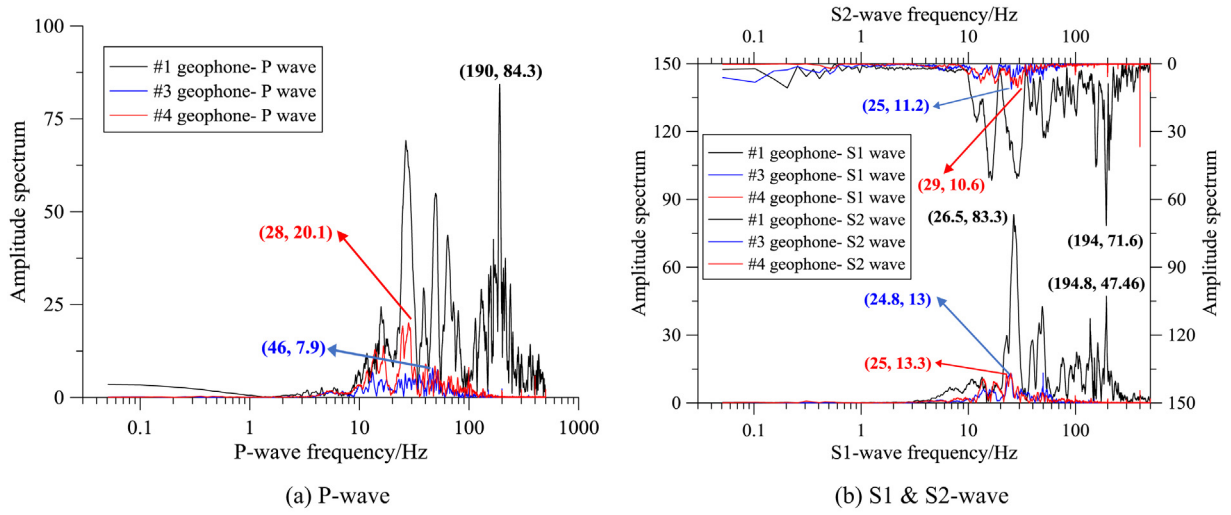

Fig. 13. Frequency-spectrum distributions of P and S-wave recorded by the #1, #3 and #4 geophones of Test 1.

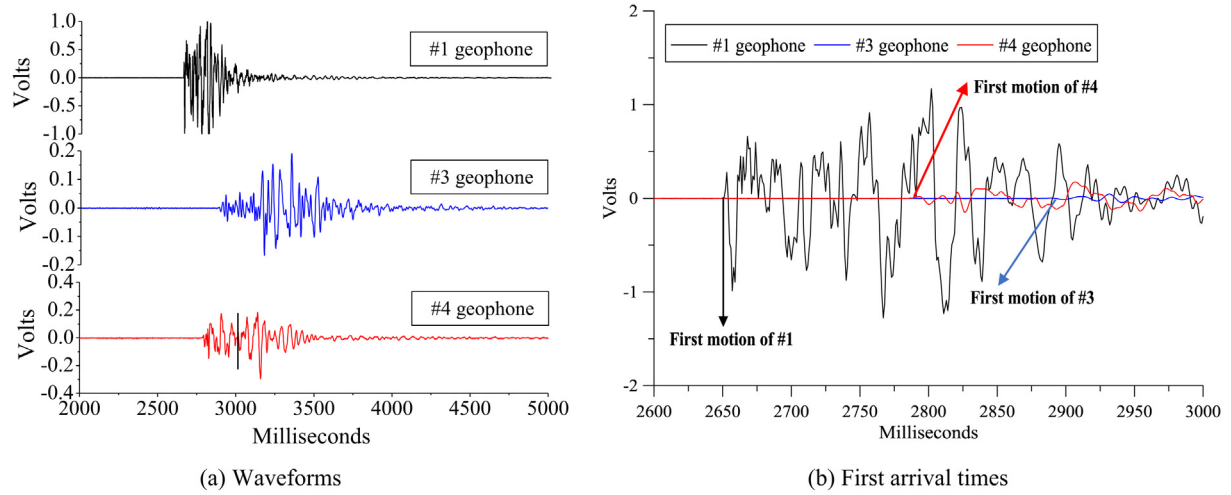

Fig. 14. Waveforms and first arrival times of S1-wave recorded by the #1, #3 and #4 geophones. Note: in the subgraph (b), the amplitudes of both #3 and #4 geophones were magnified 5 times.

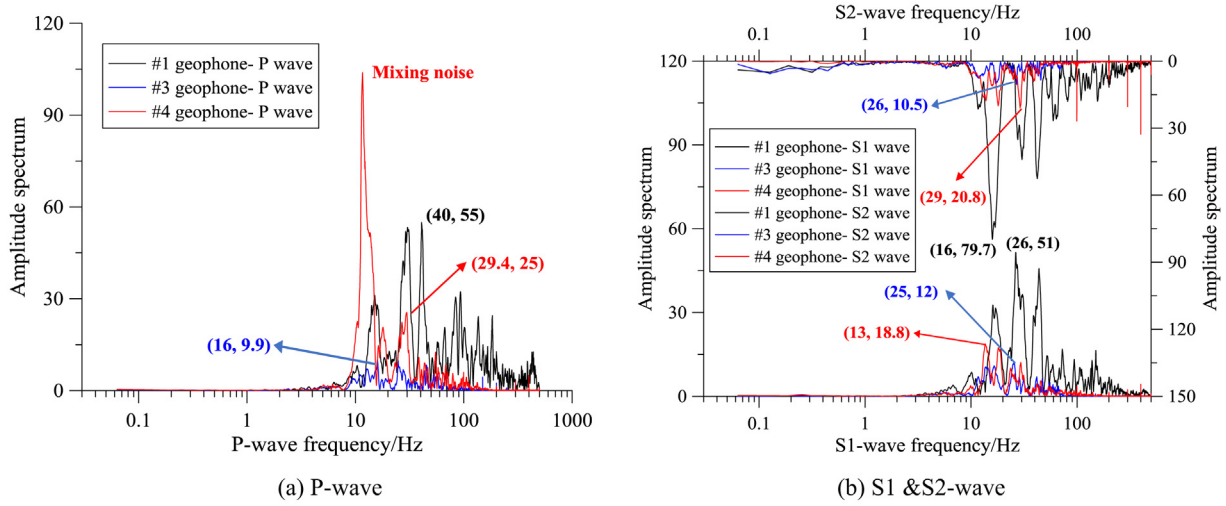

Fig. 15. Frequency-spectrum distributions of P and S-wave recorded by #1, #3 and #4 geophones of Test 2.

test. The amplitude of seismic wave decreased gradually with propagation, the high frequency signals weakened, and the low frequency signals strengthened gradually, as shown in Fig. 14(a). In particular, the waveforms collected by the #4 geophone were obviously divided into two parts: the first part was the receiving waves, and the other was the "noise" generated by surrounding rock mass rupture, which has been confirmed in laboratory observations shown in Fig. 6(a). That the low frequency signals were significantly enhanced was verified in Fig. 15(a), which was much higher than the amplitude at the dominant frequency point of other geophones, and it can obtain that the low frequency signals was generated from deformation and fracture as Fig. 6(a), and not generated from the blasting. Compared with the first arrival time of P-wave in Test 1, the first arrival time of S-wave was obviously lagged (in Fig. 14(b)) due to the relatively small difference of propagation distances. In addition, the small the propagation distance is, the earlier the first arrival time of S-wave is.

From Fig. 15(a), the vertical propagation distance of the #3 geophone increased by only 7.66 m compared with the #4 geophone, and the former experienced one more joint, but the amplitude spectrum corresponding to dominant frequency reduced by nearly 2.53 times (the test values of the two tests were very close), which fully confirmed that joints generate significant attenuation effects on P-wave. In general, the attenuation index was closely related to vertical propagation distance and the number of experienced joints. The horizontal propagation distances from the source to the #3 and #4 geophones were 1365.8 m and 912.6 m, respectively, with a difference up to 453.2 m, and while there was no significant difference between both amplitude spectrums corresponding to dominant low frequencies of the two geophones, which demonstrated that the horizontal propagation distance has no certain attenuation effect on S-wave (in Fig. 15(b)).

In summary, the results of field investigations on seismic wave propagation and attenuation in the jointed rock are as follows: (1) with propagation of seismic wave, the high frequency signals attenuate significantly, and the spectrum moves from high-frequency band to low-frequency band. Especially, the joints have significant attenuation effect on P-wave, and while the attenuation effect on S-wave is not obvious; and (2) the attenuation index of P-wave is obviously higher than that of S-wave by horizontal joints. The horizontal propagation distance has little effect on attenuation of P-wave, which is closely related to vertical propagation distance and especially the number of the experienced joints. In addition, the horizontal propagation distance has a certain effect on the attenuation of S-wave.

The conclusions drawn from the experiments and in-situ tests were in good agreement with each other. The attenuation index of P-wave was obviously higher than that of S-wave by horizontal joints, the high frequency signals of P-wave significantly weakened, and the frequency spectrum evolved from high frequency to low frequency accompanied with unobvious attenuation of S-wave. Additionally, the joints attenuated the high-frequency signals of P-wave and the low frequency components were enhanced according to the experiments, while the spectrum still showed wide frequency characteristics, and the attenuation of joints on S-wave mainly concentrated in high frequency band. In the field observation, the horizontal propagation distance had little effect on the attenuate of P-wave, while it has a certain effect on the attenuation of S-wave.

4. Conclusions

First, the propagation and attenuation rules of seismic wave in the intact and jointed rocks subjected to conventional triaxial loading condition were investigated experimentally, especially the effects of joints and beddings on the attenuation. Secondly, the attenuation characteristics of seismic wave generated by blasting in underground strata are in-situ tested, and the attenuation rules by the joints between strata is analysed. The following main conclusions are drawn:

(1) Joint can significantly reduce the velocity of seismic wave in rocks. Although bedding can attenuate the intensity of the P and S-wave, the attenuation effect on wave velocity is not obvious. For horizontal joint, it can't obviously attenuate the vertically propagating S-wave. The inclined bedding further reduces P-wave on basis of attenuation generated by the joint, and the spectrum moves to low frequency band.
(2) For sample without artificially manufactured joint, the higher the applied stress is, the weaker the attenuation effect of seismic signal is, and the higher the corresponding dominant frequency is. For jointed sample, the effect of stress on P and S-wave attenuation is not significant. The higher the applied stress is, the weaker the attenuation effect by bedding is, and the stronger the low frequency signal is. Additionally, the attenuation effect of the bedding on S-wave is weaker compared with P-wave.
(3) Based on the field investigation, joint has significant attenuation effect on seismic P-wave, but it is not obvious on S-wave, verifying the outcomes obtained from the lab. The horizontal propagation distance has little effect on the attenuation of P-wave, which is closely related to vertical propagation distance, especially the number of the experienced joints.

Acknowledgments

We gratefully wish to acknowledge the collaborative funding support from the National Natural Science Foundation of China, China (51574225), the Fundamental Research Funds for the Central Universities, China (YC150001), and a Project Funded by the Priority Academic Program Development of Jiangsu Higher Education Institutions, China (PAPD).

References

[1] S.C. Bandis, A.C. Luden, N.R. Barton, Fundamentals of rock joint deformation, Int. J. Rock Mech. Min. Sci. & Geomech. Abstr. 20 (1983) 249–268.
[2] S.R. Brown, C.H. Scholz, Closure of rock joints, J. Geophys. Res. 91 (1986) 4939–4948.
[3] N.G.W. Cook, Natural joints in rock: Mechanical, hydraulic, and seismic behavior and properties under normal stress, Int. J. Rock Mech. Min. Sci. & Geomech. Abstr. 29 (1992) 198–223.
[4] X.F. Deng, J.B. Zhu, S.G. Chen, Z.Y. Zhao, X.Y. Zhou, J. Zhao, Numerical study on tunnel damage subject to blast-induced shock wave in jointed rock masses, Tunn. Undergr. Sp. Tech. 43 (2014) 88–100.
[5] L.J. Pyrak-Nolte, Seismic Visibility of Fractures. Ph.D. thesis, University of California, 1988.
[6] L.J. Pyrak-Nolte, L.R. Myer, N.G.W. Cook, Transmission of seismic waves across natural fractures, J. Geophys. Res. 95 (1990) 8617–8638.
[7] B.L. Gu, R. Sufirez-River, K.T. Nihei, L.R. Myer, Incidence of plane waves upon a fracture, J. Geophys. Res. 101 (1996) 25337–25346.
[8] X.B. Zhao, J. Zhao, J.G. Cai, A.M. Hefny, UDEC modelling on wave propagation across fractured rock masses, Comput. Geotech. 35 (2008) 97–104.
[9] J.B. Zhu, X.F. Deng, X.B. Zhao, J. Zhao, A numerical study on wave transmission across multiple intersecting joint sets in rock masses with UDEC, Rock Mech. Rock Eng. 46 (2013) 1429–1442.
[10] C. Saroglou, V. Kallimogiannis, Fracturing process and effect of fracturing degree on wave velocity of a crystalline rock, J. Rock Mech. Geotech. Eng. 9 (2017) 797–806.
[11] X.C. Yang, K. Sasaki, X.M. Zhang, Y.C. Sugai, Permeability estimate of underground long-wall goaf from P-wave velocity and attenuation by lab-scale experiment on crushed rock samples, J. Appl. Geophys. 159 (2018) 785–794.
[12] P. Gaviglio, Longitudinal waves propagation in a limestone: the relationship between velocity and density, Rock Mech. Rock Eng. 22 (1989) 299–306.
[13] L.J. Pyrak-Nolte, L.R. Myer, N.G. W. Cook. Seismic visibility of fractures, in: The 28th U.S. Symposium on Rock Mechanics Tucson, AZ, June 29-July 1, 1987.
[14] J. Zhao, X.B. Zhao, J.G. Cai, A further study of P-wave attenuation across parallel fractures with linear deformational behaviour, Int. J. Rock Mech. Min. Sci. 43 (2006) 776–778.
[15] Z.L. Wang, H. Konietzky, R.F. Shen, Analytical and numerical study of P-wave attenuation in rock shelter layer, Soil Dyn. Earthq. Eng. 30 (2010) 1–7.
[16] P. Zakian, N. Khaji, A stochastic spectral finite element method for wave propagation analyses with medium uncertainties, Appl. Math. Model. 63 (2018) 84–108.
[17] J.C. Li, G.W. Ma, Analysis of blast wave interaction with a rock joint, Rock Mech. Rock Eng. 43 (2010) 777–787.
[18] J.C. Li, W. Wu, H.B. Li, J.B. Zhu, J. Zhao, A thin-layer interface model for wave propagation through filled rock joints, J. Appl. Geophys. 91 (2013) 31–38.
[19] W. Wu, H.B. Li, J. Zhao, Dynamic responses of non-welded and welded rock fractures and implications for P-wave attenuation in a rock mass, Int. J. Rock Mech. Min. Sci. 77 (2015) 174–181.
[20] J.G. Cai, J. Zhao, Effects of multiple parallel fractures on apparent attenuation of stress waves in rock masses, Int. J. Rock Mech. Min. Sci. 37 (2000) 661–682.
[21] E.I. Mashinskii, Elastic-microplastic nature of wave propagation in the weakly consolidated rock, J. Appl. Geophys. 101 (2014) 11–19.
[22] L.F. Fan, G.W. Ma, J.C. Li, Nonlinear viscoelastic medium equivalence for stress wave propagation in a jointed rock mass, Int. J. Rock Mech. Min. Sci. 50 (2012) 11–18.
[23] F.L. Fan, H.Y. Sun, Seismic wave propagation through an in-situ stressed rock mass, J. Appl. Geophys. 121 (2015) 13–20.
[24] F.L. Fan, L.J. Wang, Z.J. Wu, Wave transmission across linearly jointed complex rock masses, Int. J. Rock Mech. Min. Sci. 112 (2018) 193–200.
[25] G.W. Ma, F.L. Fan, J.C. Li, Evaluation of equivalent medium methods for stress wave propagation in jointed rock mass, Int. J. Numer. Anal. Met. 37 (2013) 701–715.
[26] D. Pandolfi, C.J. Bean, G. Saccorotti, Coda wave interferometric detection of seismic velocity changes associated with the 1999 M = 3.6 event at Mt, Vesuvius. Geophys. Res. Lett. 33 (2006) L06306.
[27] R. Snieder, A. Gret, H. Douma, J. Scales, Coda wave interferometry for estimating nonlinear behavior in seismic velocity, Science 295 (2002) 2253–2255.
[28] M.M. Scuderi, C. Marone, E. Tinti, G. Di Stefano, C. Collettini, Precursory changes in seismic velocity for the spectrum of earthquake failure modes, Nat. Geosci. 9 (2016) 695–700.
[29] V.A. Korneev, S. Glubokovskikh, Seismic velocity changes caused by an overburden stress, Geophysics 78 (2013) Wc25-Wc31.
[30] H.S. Jia, E. Wang, D.Z. Song, X.R. Wang, M. Ali, Precursory changes in wave velocity for coal and rock samples under cyclic loading, Results Phys. 12 (2019) 432–434.
[31] L.H. Adams, E.D. Williamson, The compressibility of minerals and rocks at high pressures, J. Franklin I. 195 (1923) 475–529.
[32] E.C. David, R.W. Zimmerman, Elastic moduli of solids containing spheroidal pores, Int. J. Eng. Sci. 49 (2011) 544–560.
[33] R.L. Morris, D.R. Grine, T.E. Arkfeld, Using compressional and shear acoustic amplitude for the location of fractures, J. Petr. Technol. 6 (1964) 623–632.
[34] R.L. Kleinberg, E.Y. Chow, T.J. Plona, M. Orton, W.J. Canady, Sensitivity and reliability of fracture detection techniques for borehole application, J. Petr. Technol. 4 (1982) 657–663.
[35] W.L. Medlin, L. Marsi, Laboratory experiments in fracture propagation, Soc. Pet. Engr. J. 24 (1984) 256–268.
[36] M.S. King, L.R. Myer, J.J. Rezowalli, Experimental studies of elastic-wave propagation in a columnar-jointed rock mass, Geophys. Prospect. 8 (1986) 1185–1199.
[37] H.Y. Wang, A. Dyskin, E. Pasternak, P. Dight, M. Sarmadivaleh, Effect of the intermediate principal stress on 3-D crack growth, Eng. Fract. Mech. 204 (2018) 404–420.
[38] L.J. Pyrak-Nolte, The seismic response of fractures and the interrelations among fracture properties, Int. J. Rock Mech. Min. Sci. Geomech. Abstr. 33 (1996) 785–802.
[39] A.V. Dyskin, L.N. Germanovich, K.B. Ustinov, Asymptotic solution for long cracks emanated from a pore in compression, Int. J. Fract. 62 (4) (1993) 307–324.